THE ASTROPHYSICAL JOURNAL, 450:51–63, 1995 September 1

THE SOFT X-RAY PROPERTIES OF A LARGE OPTICAL QSO SAMPLE: *ROSAT* OBSERVATIONS OF THE LARGE BRIGHT QUASAR SURVEY

PAUL J. GREEN,[1,2] NORBERT SCHARTEL,[3] SCOTT F. ANDERSON,[4] PAUL C. HEWETT,[5] CRAIG B. FOLTZ,[6]
WOLFGANG BRINKMANN,[3] HENNER FINK,[3] JOACHIM TRÜMPER,[3] AND BRUCE MARGON[4]
Received 1994 October 20; accepted 1995 March 14

ABSTRACT

Of the more than 1000 QSOs in the Large Bright Quasar Survey (LBQS), we study the X-ray properties of 908 that were covered by the *ROSAT* All-Sky Survey (RASS). These data constitute among the largest, most homogeneous X-ray surveys of QSOs to date, and as such are well suited to the study of the multiwavelength properties of QSOs. Due to the ≈ 600 s RASS exposure times, only 10% of the QSOs are detected in X-rays. However, by stacking X-ray counts, we obtain effectively much more sensitive observations for an *average* QSO in bins of redshift or luminosity, and for several classes of QSOs. We confirm a correlation of α_{ox} with luminosity for the overall sample. For higher redshifts and optical luminosities, radio-loud QSOs appear to become progressively more luminous in X-rays than radio-quiet QSOs. The X-ray properties of a subsample of 36 broad absorption line QSOs suggest that they are strongly absorbed or underluminous in the X-rays, while a subsample of 22 Fe II–strong QSOs is anomalously X-ray bright.

Subject headings: galaxies: active — quasars: general — surveys — X-rays: galaxies

1. INTRODUCTION

The *ROSAT* X-ray satellite (Trümper 1983) was launched in 1990 June, and soon after began the first all-sky soft X-ray survey. The *ROSAT* All-Sky Survey (RASS) benefits from the low intrinsic background of the Position Sensitive Proportional Counter (PSPC; Pfeffermann et al. 1987), and the large collecting area and field of view of the *ROSAT* telescope (Aschenbach 1988). The RASS provides X-ray information (detections or upper limits) for several thousand previously cataloged quasi-stellar objects (hereafter QSOs). Such data are relevant to X-ray luminosity functions, the X-ray evolution of QSOs, and the contribution of QSOs to the X-ray background (XRB). The relationship between the X-ray and other wavelength regimes elucidates the nature, origin, and energetics of continuum and emission-line processes in QSOs. Detailed multiwavelength studies of individual objects can be very revealing, but large samples permit sound statistical tests that place more anecdotal results in context.

X-ray observations of samples selected in other wave bands (e.g., optical or radio) provide information complementary to X-ray–selected samples (e.g., Bade et al. 1992; Franceschini et al. 1994). For instance, the Shanks et al. (1991) optical followup of X-ray sources in a 30 ks *ROSAT* PSPC image revealed about 10% more QSOs than were cataloged in a UV excess (UVX) survey of the same field to $B \leq 21$ (Boyle et al. 1990). On the other hand, four of 16 UVX QSOs remained undetected by *ROSAT*. This illustrates that all QSO samples suffer from some incompleteness and/or selection effects. Nevertheless, combinations of automated selection techniques have recently led to optically selected QSO samples that are remarkably well defined and quantifiable. Extensive catalogs of faint QSOs (e.g., Warren, Hewett, & Osmer 1994; Boyle et al. 1990; Koo, Kron, & Cudworth 1986) have proved useful for studies of space densities and evolution, but are too faint for detailed optical spectra or detection in wave bands other than the optical using reasonable exposure times. The Bright QSO Survey of Schmidt & Green (1986) is a well-studied exception, but one that is dominated by low-redshift QSOs. Furthermore, that sample is too small (≈ 100 objects) to provide statistically valuable samples of specific classes of QSOs (e.g., broad absorption-line, radio-loud, or strong Fe II QSOs).

To take advantage of the unique attributes of the RASS (e.g., over previous *Einstein* observations), a homogeneous optical QSO sample ideally would be (1) large, with a wide range of redshifts and luminosities; (2) selected from extensive areal sky coverage; (3) apparently bright, so that a significant fraction will be detected or have sensitive upper limits in the RASS; (4) uniformly selected, with quantifiable selection criteria so that selection biases are well understood; (5) complemented by homogeneous, high-quality data in other wave bands. Such a sample, the Large Bright Quasar Survey (LBQS, described in the next section) has been partly characterized in X-rays by Margon et al. (1992) using 146 LBQS QSOs observed by *Einstein*. The RASS data now enable us to study the X-ray properties of nearly the entire LBQS sample, permitting further division into specific subsamples. Section 2 outlines the *ROSAT* data and our X-ray analysis. We discuss the optical-to-X-ray properties of the full sample in § 4. Three subsamples—radio-loud, broad absorption-line, and Fe II–strong QSOs—are compared to appropriate control samples in the following three sections, followed by our conclusions in § 8. The statistical techniques we employ are detailed in an appendix.

2. THE LBQS QSO SAMPLE

The Large Bright Quasar Survey (Hewett, Foltz, & Chaffee 1995; Morris et al. 1991; Chaffee et al. 1991; Hewett et al. 1991; Foltz et al. 1987, 1989) is a large, uniformly selected sample of QSOs with a wide range of redshifts. LBQS QSO

[1] Harvard-Smithsonian Center for Astrophysics, 60 Garden Street, Cambridge, MA 02138.
[2] Hubble Fellow.
[3] Max Planck Institut für extraterrestrische Physik, Giessenbachstraße 1, D-85740 Garching bei München, Germany.
[4] Astronomy Department, University of Washington, Seattle, WA 98195.
[5] Institute of Astronomy, University of Cambridge, Madingley Road, Cambridge, England CB3 0HA, UK.
[6] Multiple Mirror Telescope Observatory, University of Arizona, Tucson, AZ 85721.

candidates were selected using the Automatic Plate Measuring Machine (APM; see Irwin & Trimble 1984) to scan UK Schmidt direct photographic and objective prism plates (see Hewett et al. 1985 for a description of the objective prism plate scanning procedures and the basic selection algorithms). A combination of quantifiable selection techniques was used, including color selection, selection of objects with strong emission lines, selection of objects having redshift absorption features or continuum breaks. As described in the series of LBQS papers, the technique appears to be highly efficient at finding QSOs with $0.2 < z < 3.3$, a significantly broader range than past work. Follow-up (6–10 Å resolution) optical spectra with S/N $\approx$ 10 in the continuum at 4500 Å were obtained at the MMT and 2.5 m duPont telescopes.

The entire LBQS optical sample here consists of 1056 QSOs over more than 450 deg^2 of the sky, with $16.0 \leq B_J \leq 18.9$. All 18 fields included in the LBQS were surveyed to $B_J = 18.41$, although the deepest field extended to $B_J = 18.85$. Most of the LBQS QSOs are sufficiently bright that even the RASS nondetections contribute useful information on the *average* X-ray properties of QSOs. Redshifts range from 0.2 to 3.4, with a mean of 1.3. The low-redshift cutoff was arbitrarily imposed on the LBQS to avoid spatially extended objects that otherwise meet the selection criteria.

The large sample size of the LBQS offers several advantages. First, one can average QSOs in relatively fine bins of optical luminosity or redshift, while maintaining enough objects per bin to allow a meaningful determination of *average* QSO X-ray properties as a function of redshift and optical luminosity. Since Galactic hydrogen column density, N_H (together with X-ray spectral slope) determines X-ray counts-to-flux conversion factors, the ability to bin in N_H provides a valuable check on the influence of N_H on our samples. Second, relatively rare types of QSOs are present in large numbers; for example, there are over 30 broad absorption line (hereafter BAL) QSOs in the LBQS.

For ease of comparison with other work, we convert optical magnitudes originally in the B_J band to the B band using $B = B_J + 0.28(B-V)$ (Blair & Gilmore 1982), assuming $B-V = 0.3$. We apply a correction for extinction using the results of Burstein & Heiles (1978, 1982) and assuming $A_B = 4.0E(B-V)$. The fit of Fisher & Tully (1981) is used where the Burstein & Heiles data are not reliable. Our extinction-corrected apparent blue magnitudes thus have a mean of 18.2. We make no correction to the optical magnitudes for emission lines. Such a correction will vary with redshift and between QSOs, but in the mean would represent an increase of $\approx$0.2 to the B_J magnitudes of QSOs with $z < 3$.

Composite QSO spectra (Francis et al. 1991; Cristiani & Vio 1990) show optical slopes between -0.3 and -0.7, with quoted errors of ± 0.2). We calculate the K-corrections and conversions between different rest-frame wavelengths by assuming an intrinsic optical spectrum $f_\nu \propto \nu^{-0.5}$. Throughout this paper, luminosities are calculated assuming $H_0 = 50$ km s^{-1} Mpc^{-1} and $q_0 = 0.5$, with specific optical normalization from Marshall et al. (1984).

Even though the LBQS QSOs are *apparently* bright, objects in substantial numbers are represented over a very wide range of absolute magnitudes, $-22 < M_B < -28.6$. This corresponds to optical (rest frame 2500 Å) luminosities from 29.4 to 32.0 in the logarithm, a factor of about 400 in intrinsic optical power. The mean log l_{opt} of the LBQS/RASS sample is 30.9 ± 0.5.

3. *ROSAT* OBSERVATIONS AND DETECTION CRITERIA

The Position Sensitive Proportional Counter (PSPC) of the *ROSAT* X-ray satellite performed an All-Sky Survey (hereafter RASS) in the soft X-ray band (0.1–2.4 keV) between 1990 August and 1991 February. A typical limiting flux for source detection ($\approx 4\ \sigma$) is a few times 10^{-13} ergs cm^{-2} s^{-1}, depending on the actual N_H value and the spectral slope of the source.

We removed from consideration all LBQS QSOs within 1°.72 of the approximate X-ray center of the Virgo Cluster, since this region is contaminated by strong extended cluster emission. To ensure that background estimation would be of sufficient quality, we adopted 300 s as a minimum *ROSAT* exposure time for inclusion in our sample, a criterion that excludes 20 QSOs. Exposure times thus range from 300 to 690 s, with a mean of 560 s. Of the 1056 LBQS QSOs here, two lack reliable B_J magnitudes due to image overlap. We also excluded data from regions with uncertain aspect solutions; this excludes 82 QSOs mostly in LBQS fields 0300+0000 and 1240+0000. Our photon positional data are thus subject only to random errors, of order 5″–7″. Exclusion of the Virgo region and QSOs near other extended or unrelated X-ray bright sources removes a further 44 QSOs from the sample. This leaves 908 QSOs comprising the LBQS/RASS sample. Basic properties of the LBQS/RASS sample are illustrated in Figure 1.

The high galactic latitude of the LBQS fields together with the typical RASS exposure times result in a RASS source density sufficiently low that simple X-ray aperture photometry is adequate. To measure the mean background, an annulus from 600″ to 1200″ provides adequate background flux but completely avoids the wings of bright source point spread functions. Any source found by the *ROSAT* Extended Scientific Analysis System (EXSAS; Zimmerman et al. 1993) to have maximum likelihood 6 or greater ($M/L = -\ln p$) we excise

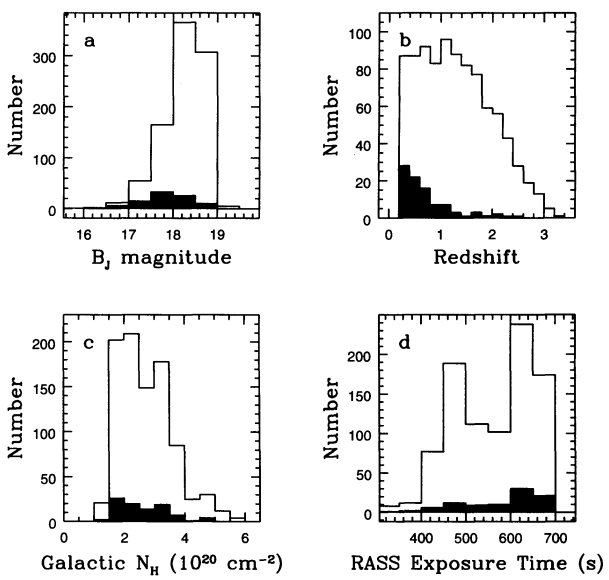

FIG. 1.—Basic properties of the LBQS/RASS sample. Histograms of the entire LBQS/RASS sample (*open*) and the X-ray detections only (*shaded*). Sample includes 908 QSOs with RASS data uncontaminated by nearby unrelated sources and with exposure times $\geq$300 s. (*a*) B_J magnitudes from the APM direct plates. (*b*) Redshift. (*c*) Galactic hydrogen column density from Stark et al. (1992). (*d*) Exposure time in the *ROSAT* All-Sky Survey.

from this background region. We determined the optimal source aperture for high signal-to-noise ratio (SNR) as follows: using a preliminary list of LBQS/RASS $M/L > 10$ detections, we calculated the average SNR for 24 different source apertures with radii from 50″ to 400″. Since a broad maximum appears centered at 180″, we have adopted this as the optimal aperture radius for faint sources in the RASS.

Next, by cross-correlating $M/L = 6$ EXSAS detections with the LBQS positions, we empirically determined the maximum optimal X-ray/optical distance for accepting a positional coincidence. The distance at which the histogram of total source coincidences reaches a minimum before rising again (due to an increasing number of unrelated coincidences) is 50″, which corresponds well to the PSPC positional errors in the RASS. We therefore require the separation between the X-ray and optical positions to be less than 50″. To avoid any possibility of contamination, we also eliminate (22) LBQS QSOs that had an $M/L = 6$ EXSAS detection in the source aperture between 50″ and 180″.

The raw source count rate is $R_{\rm src} = (C_{\rm tot} - C^s_{\rm bkg})/T$, where $C_{\rm tot}$ is the total number of counts in the source aperture and $C^s_{\rm bkg}$ is the number of counts in the background annulus, normalized by the ratio of source area to background area A^s/A^b. The error in count rate for the source may be expressed in terms of the area-normalized count rates, $R_{\rm src}$ and $R^s_{\rm bkg}$ and the exposure time T, as

$$\sigma_{\rm src} = \sqrt{\frac{R_{\rm src} + (1 + A^s/A^b)R^s_{\rm bkg}}{T}} .$$

We have also determined an aperture correction factor from the source count rate as a function of source aperture radius, using a dozen bright QSOs observed in the RASS. At an aperture radius of about 400″, the source counts reach a maximum 1.28 times larger than measured in our optimal 180″ radius aperture. We find a dispersion of 0.08 in this factor for sources with $1.3 < \Gamma < 3.4$, and no correlation with the X-ray photon index. Thus, we multiply all X-ray fluxes and luminosities by this factor.

In determining the optimal threshold for source detection, two types of contamination of the *ROSAT* LBQS observations were considered—the chance coincidence of unrelated X-ray sources, and random background fluctuations. Both increase the contamination of *ROSAT*-detected objects as the detection threshold is lowered. The most reliable way to estimate the contamination from both causes is to run the detection algorithm both at the actual (optical) LBQS positions and for a comparably sized control sample. We generated a control sample of 710 positions at least 6′ away from any optical QSO position in LBQS field 1140+0000. This plate is in a region of typical $N_{\rm H}$ and has average RASS exposure. We have selected as a detection criterion that $C_{\rm src} \geq 4(C^s_{\rm bkg})^{1/2}$, where $C_{\rm src}$ and $C^s_{\rm bkg}$ are the number of raw source and background counts in the source aperture. Since only three positions in the control sample were "detected" by this criteria, we estimate a spurious detection rate of less than 5%. Our criterion corresponds approximately to $R_{\rm src} \geq 2.3\ \sigma_{\rm src}$, where $R_{\rm src}$ and $\sigma_{\rm src}$ are the source count rate and its error, respectively. Such a detection threshold is justified in studies such as this, where X-ray–emitting objects are known from optical selection to exist at these positions a priori.

Of the 908 QSOs in the LBQS/RASS sample, 92 are detected in X-rays by our criteria. For the nondetections, we assign an upper limit of $4(C^s_{\rm bkg})^{1/2}$ to the raw counts. For two close QSOs (0048+0029 and 0048+0025), we use their (single) detection as an upper limit but exclude them in the stacking procedure described in § A2. X-ray broadband fluxes are derived for each QSO from RASS counts and galactic hydrogen column density ($N_{\rm H}$) using standard counts-to-flux conversion factors (*ROSAT* Technical Appendix 1991), an assumed photon index, and $N_{\rm H}$ values interpolated from Stark et al. (1992). $N_{\rm H}$ values in the LBQS/RASS range from 1.3 to 5.6×10^{20} cm^{-2}, with a mean of 2.74, yielding typical conversion factors near 2×10^{-11} counts^{-1} ergs cm^{-2}. We use a mean *ROSAT* (0.1–2.4 keV) photon index of $\Gamma = 2.7$ for known radio-quiet (RQ) QSOs, and $\Gamma = 2.1$ for known radio-loud (RL) QSOs. These classes are defined below in § 5. For QSOs with no radio data, we use $\Gamma = 2.5$. All these values are as derived by Schartel et al. (1995) using the same LBQS/RASS samples and data. We note that in one common notation (e.g., Wilkes et al. 1994), the X-ray spectral energy index α is defined by $f_\nu \propto \nu^{-\alpha}$ (so that $\alpha = \Gamma - 1$). About 10% of the objects with no radio data may be radio-loud quasars. For these, the assumption of $\Gamma = 2.5$ differs significantly from the correct mean photon index, but the resulting flux discrepancies have an entirely negligible effect on the results presented here. We calculate monochromatic X-ray luminosities log l_x (and corresponding upper limits) at 2 keV in the rest frame, using the photon indices described above. The combined uncertainty in the flux of an individual QSO due to $N_{\rm H}$ interpolation, uncertainty in Γ, and counts-to-flux conversion calibrations is $\lesssim 30\%$.

As expected, the mean redshift of the 92 detected QSOs is significantly lower than for nondetections (0.74 vs. 1.36), and their mean B_J is brighter (17.8 vs. 18.3, see Figs. 1*a*–1*b*). The fraction of QSOs detected as a function of $N_{\rm H}$ is $\approx 10\%$ for $N_{\rm H} \leq 5 \times 10^{20}$ (see Fig. 1*c*). Since only 2% of the LBQS/RASS sample have Galactic column densities larger than this, and since the $N_{\rm H}$ distributions of detections and nondetections are not significantly different in two-sample tests, we conclude that Galactic $N_{\rm H}$ does not strongly affect the detection probability in the LBQS/RASS sample.

Detected objects span a (0.1–2.4 keV) flux range of 0.6–7×10^{-12} with a mean of 1.4×10^{-12} ergs cm^{-2} s^{-1}. The lowest (most sensitive) flux upper limit in the sample is 5.4×10^{-13} ergs cm^{-2} s^{-1}. The peak of the flux histogram is at about 10^{-12} ergs cm^{-2} s^{-1}, and this should approximately correspond to the X-ray flux completeness limit for LBQS QSOs in the RASS. This limit is a function of the RASS exposure time, which has a bimodal histogram for the LBQS fields, with two peaks centered near 500 and 650 s (Fig. 1*d*). Thus, the quoted X-ray flux limit, although indicative, is not strictly applicable to all fields of the LBQS. In any case, the bulk of our analysis is based on stacking (see § A2 below), which obviates the distinction between detections and nondetections by summing counts from all QSOs within chosen groupings or bins.

For the 92 LBQS/RASS detections, Table 1 contains the X-ray and optical data, with luminosities calculated as described in the text. Table 1 is published in its entirety in computer-readable form in the AAS CD-ROM Series, Vol. 5. Columns in Table 1 are as follows: (1) name of the LBQS QSO, (2) redshift, (3) B_J magnitude, (4) extinction A_B, in magnitudes, (5) Galactic hydrogen column density $N_{\rm H}$ in units 10^{20} cm^{-2}, (6) RASS source counts $C_{\rm src}$, (7) RASS background counts normalized to the source aperture area, $C^s_{\rm bkg}$, (8) RASS exposure time T, (9) logarithm of the X-ray luminosity in ergs s^{-1}

TABLE 1

RAW DATA AND LUMINOSITIES OF DETECTED LBQS/RASS QSOs

Name (1)	z (2)	B_J (3)	A_B (4)	N_H (5)	C_{src} (6)	C^s_{bkg} (7)	T (8)	log l_x (9)	log l_{opt} (10)	α_{ox} (11)	Notes (12)
0002−0149	1.705	18.7	0.10	3.5	22.0 ± 7.7	16.5 ± 0.6	565.7	28.11	31.09	1.14	RL[a]
0003+0146	0.235	16.6	0.04	3.2	138.7 ± 16.3	20.6 ± 0.6	626.1	26.77	30.22	1.32	
0004+0036	0.317	17.8	0.08	2.9	63.1 ± 11.2	18.8 ± 0.6	630.7	26.69	30.01	1.28	
0004+0224	0.301	17.3	0.04	3.2	70.8 ± 12.8	22.4 ± 0.6	658.3	26.69	30.15	1.33	
0018−0004	1.110	18.1	0.04	2.8	19.5 ± 8.0	17.7 ± 0.7	624.2	27.44	30.95	1.35	
0019−0000	0.578	18.3	0.04	3.2	27.2 ± 8.8	19.1 ± 0.7	617.1	26.96	30.31	1.29	
0020−0300	0.742	17.3	0.03	3.0	30.9 ± 8.8	16.4 ± 0.6	573.5	27.28	30.92	1.40	Fe
0020+0058	0.730	18.0	0.02	3.2	18.6 ± 7.6	17.7 ± 0.6	639.0	27.01	30.63	1.39	
0020+0018	0.421	18.6	0.02	3.1	25.6 ± 8.3	18.1 ± 0.6	632.5	26.59	29.91	1.27	
0022+0015	0.399	16.9	0.00	2.9	41.6 ± 10.2	17.1 ± 0.6	630.5	26.72	30.54	1.47	
0022−0140	0.773	18.3	0.02	2.8	24.5 ± 8.5	16.9 ± 0.6	582.7	27.19	30.55	1.29	
0028−0131	0.672	17.4	0.03	2.8	24.4 ± 8.6	19.9 ± 0.6	650.5	26.99	30.80	1.46	
0040−2917	2.090	17.8	0.06	1.8	17.0 ± 7.3	16.2 ± 0.6	497.8	27.97	31.61	1.40	RQ
0042−2550	0.455	18.3	0.03	1.3	25.9 ± 8.3	19.4 ± 0.6	481.0	26.51	30.10	1.38	
0042−2729	0.930	18.7	0.00	1.5	17.4 ± 7.6	18.3 ± 0.6	491.3	27.10	30.54	1.32	
0050−2742	0.480	17.9	0.06	1.6	39.0 ± 9.3	17.4 ± 0.6	499.1	26.79	30.32	1.35	
0051−0146	0.408	17.7	0.07	3.6	24.3 ± 6.7	8.0 ± 0.4	345.7	26.85	30.26	1.31	
0052−0015	0.648	17.7	0.03	3.0	23.7 ± 7.3	11.7 ± 0.5	438.0	27.14	30.65	1.35	
0053+0124	0.441	17.8	0.08	3.1	17.9 ± 7.1	13.3 ± 0.5	516.7	26.57	30.29	1.43	
0055+0225	0.373	18.6	0.05	3.2	22.9 ± 8.0	15.7 ± 0.6	628.8	26.43	29.82	1.30	
0056−0009	0.718	17.7	0.02	3.2	25.8 ± 8.1	13.0 ± 0.5	525.2	27.34	30.73	1.30	RL[a]
0056+0009	0.613	18.0	0.07	3.0	28.4 ± 8.2	13.9 ± 0.5	541.9	27.07	30.49	1.31	
0100−2702	1.599	17.9	0.10	1.9	24.6 ± 8.2	19.9 ± 0.6	501.0	27.99	31.36	1.29	RL[a]
0100+0205	0.395	17.5	0.01	2.9	40.3 ± 9.6	19.7 ± 0.6	641.6	26.70	30.29	1.38	
0101−2611	0.278	18.0	0.07	1.9	61.0 ± 11.4	18.9 ± 0.6	492.4	26.51	29.81	1.27	
0102−2713	0.779	17.5	0.06	1.9	18.3 ± 7.5	20.5 ± 0.6	492.7	27.02	30.89	1.49	Fe
0102−0147	0.574	17.4	0.09	4.0	20.8 ± 7.5	13.3 ± 0.5	632.4	26.89	30.68	1.46	Fe
0103+0024	1.071	17.4	0.06	3.4	21.8 ± 9.3	17.9 ± 0.6	639.7	27.51	31.21	1.42	
0103−2622	0.776	16.9	0.06	1.9	24.8 ± 8.3	20.3 ± 0.6	493.9	27.13	31.13	1.53	
0106+0119	2.101	18.3	0.02	3.1	29.8 ± 9.0	22.8 ± 0.6	640.8	28.37	31.39	1.16	RL[a]
0107−0235	0.956	18.1	0.10	4.1	65.3 ± 11.8	15.4 ± 0.6	648.3	27.98	30.85	1.10	RL[a], Fe
0109+0242	0.263	18.4	0.07	3.0	17.1 ± 6.9	13.9 ± 0.5	635.3	25.94	29.60	1.41	
1010−0056	0.202	18.3	0.07	3.6	27.8 ± 8.4	20.1 ± 0.7	634.8	25.96	29.41	1.32	
1013+0124	0.783	16.6	0.03	3.6	26.8 ± 8.3	18.1 ± 0.6	613.8	27.40	31.25	1.48	RL
1021−0236	1.010	17.8	0.05	4.5	23.8 ± 8.2	19.7 ± 0.6	674.1	27.55	30.99	1.32	
1023−0040	1.750	18.6	0.08	4.7	19.6 ± 8.3	16.3 ± 0.6	634.7	28.11	31.15	1.17	
1024−0116	0.323	18.2	0.08	4.7	33.9 ± 9.2	18.8 ± 0.6	667.4	26.56	29.87	1.27	
1025−0030	2.853	18.5	0.11	4.9	18.5 ± 7.6	17.9 ± 0.6	671.7	28.62	31.60	1.14	
1130+0018	1.254	18.2	0.05	2.8	20.7 ± 8.8	23.1 ± 0.6	644.2	27.54	31.02	1.33	RQ
1135+0044	0.803	17.4	0.04	2.5	31.2 ± 9.7	26.2 ± 0.7	650.3	27.15	30.95	1.46	RQ, Fe
1137+0051	0.872	18.3	0.03	2.4	21.2 ± 8.6	25.9 ± 0.7	641.3	27.16	30.66	1.34	
1138+0204	0.386	17.6	0.03	2.4	22.0 ± 8.2	24.0 ± 0.7	647.8	26.34	30.24	1.50	RA
1140+0228	0.453	18.2	0.03	2.3	27.7 ± 8.8	24.2 ± 0.7	653.2	26.58	30.14	1.37	
1141+0227	0.210	17.7	0.04	2.2	60.9 ± 13.1	24.1 ± 0.7	646.7	26.04	29.68	1.40	RQ
1144+0140	2.585	18.5	0.04	2.3	20.9 ± 8.8	23.9 ± 0.7	645.8	28.33	31.49	1.21	
1146−0128	0.461	16.6	0.03	2.3	61.6 ± 11.6	21.5 ± 0.6	570.8	26.89	30.79	1.50	RQ
1148−0007	1.979	17.3	0.03	2.2	33.4 ± 9.0	23.1 ± 0.7	576.4	28.32	31.75	1.32	RL
1205+1729	0.547	17.2	0.11	2.5	30.6 ± 9.6	25.2 ± 0.7	669.6	26.73	30.73	1.54	RQ
1206+1716	1.014	18.2	0.10	2.6	28.6 ± 9.2	25.8 ± 0.7	675.5	27.37	30.86	1.34	RQ
1211+0848	0.817	18.0	0.00	1.5	38.3 ± 10.8	33.4 ± 0.8	639.7	27.37	30.71	1.28	RL
1211+1153	1.180	18.4	0.02	2.3	29.0 ± 10.1	28.3 ± 0.7	630.9	27.61	30.87	1.25	
1211+0841	0.583	17.8	0.00	1.5	45.0 ± 10.9	32.6 ± 0.8	641.3	26.80	30.50	1.42	RQ, Fe
1212+0945	0.378	18.4	0.00	1.6	35.5 ± 10.7	31.9 ± 0.8	637.8	26.40	29.89	1.34	
1214+0826	0.345	17.5	0.00	1.5	148.5 ± 16.3	28.3 ± 0.7	648.6	26.78	30.17	1.30	RQ
1216+1032	0.544	17.8	0.00	1.9	48.5 ± 11.0	30.6 ± 0.7	659.2	26.82	30.44	1.39	RQ
1218+1611	0.231	17.9	0.03	2.4	58.1 ± 11.6	28.7 ± 0.7	651.4	26.14	29.68	1.36	RQ
1220+0939	0.682	17.8	0.00	1.8	29.7 ± 9.3	31.8 ± 0.7	649.2	26.83	30.64	1.46	RQ, Fe
1222+0901	0.530	17.7	0.00	1.7	29.9 ± 10.2	34.7 ± 0.8	656.1	26.55	30.46	1.50	RQ
1228+1738	0.403	18.9	0.02	2.3	25.6 ± 9.5	31.3 ± 0.8	681.4	26.42	29.75	1.28	
1230+0947	0.420	16.0	0.00	1.8	127.4 ± 15.8	44.2 ± 1.0	655.8	26.95	30.94	1.53	RQ
1231+1728	0.621	18.4	0.03	2.2	32.5 ± 10.7	31.1 ± 0.8	678.7	26.94	30.33	1.30	
1238+1006	1.040	17.9	0.01	1.7	44.5 ± 12.1	46.3 ± 1.0	646.3	27.45	30.96	1.35	RQ
1238+1401	0.650	18.4	0.04	2.3	31.1 ± 10.4	38.6 ± 0.8	676.2	26.99	30.37	1.30	
1240+1746	0.547	18.1	0.00	1.8	27.8 ± 9.6	35.2 ± 0.9	679.1	26.67	30.33	1.40	
1241+1228	0.320	17.7	0.00	2.4	27.4 ± 10.1	38.0 ± 0.8	670.4	26.12	30.03	1.50	RQ

TABLE 1—*Continued*

Name (1)	z (2)	B_J (3)	A_B (4)	N_H (5)	C_{src} (6)	C^s_{bkg} (7)	T (8)	log l_x (9)	log l_{opt} (10)	α_{ox} (11)	Notes (12)
1242+1749	0.265	17.8	0.00	1.8	91.8 ± 14.2	35.2 ± 0.9	681.5	26.33	29.82	1.34	RQ
1243+1701	0.457	17.7	0.05	1.9	33.9 ± 10.5	34.5 ± 0.8	669.0	26.47	30.35	1.49	RQ
1244+1329	0.510	17.0	0.05	2.2	89.7 ± 14.0	36.7 ± 0.8	666.3	27.07	30.73	1.40	RQ
1308+0047	0.429	18.6	0.04	1.8	25.5 ± 8.4	19.4 ± 0.6	451.1	26.58	29.93	1.29	
1317−0142	0.226	17.3	0.01	2.0	33.7 ± 9.0	17.1 ± 0.5	463.1	25.95	29.89	1.51	RQ
1317−0018	0.351	17.8	0.02	1.9	25.7 ± 8.0	17.4 ± 0.6	403.3	26.30	30.08	1.45	RQ
1334−0005	0.301	18.1	0.00	1.9	18.8 ± 7.5	16.3 ± 0.5	404.2	26.15	29.81	1.40	
1338−0030	0.387	17.2	0.04	2.0	27.8 ± 8.1	17.2 ± 0.6	501.0	26.36	30.40	1.55	RQ
1338−0038	0.235	17.9	0.04	2.1	46.9 ± 10.3	18.3 ± 0.6	539.7	26.22	29.69	1.33	
1339+0210	0.270	17.9	0.01	1.8	16.7 ± 7.6	17.0 ± 0.6	400.8	25.98	29.80	1.47	
1340−0038	0.330	17.0	0.04	2.1	28.0 ± 8.4	19.3 ± 0.6	594.6	26.15	30.35	1.61	RQ
1342−0000	0.243	17.8	0.04	1.9	56.8 ± 11.1	24.2 ± 0.8	573.9	26.14	29.76	1.39	RQ
1348+0118	1.077	17.0	0.02	2.0	28.1 ± 8.9	25.9 ± 0.7	560.4	27.41	31.36	1.51	RQ
1433−0016	0.320	17.8	0.12	3.4	18.8 ± 8.0	18.4 ± 0.6	491.1	26.32	30.03	1.42	
1435−0134	1.310	16.0	0.12	3.6	26.2 ± 8.4	18.1 ± 0.6	500.5	27.99	31.96	1.53	RL
1441+0142	0.294	17.2	0.13	3.3	39.8 ± 10.0	20.0 ± 0.6	526.9	26.46	30.21	1.44	RQ
2114−4335	1.320	17.9	0.08	3.8	18.4 ± 8.3	19.9 ± 0.6	639.0	27.69	31.19	1.34	
2129−4624	0.440	17.9	0.04	3.2	36.7 ± 10.5	27.6 ± 0.7	610.9	26.82	30.24	1.31	
2154−1908	1.648	18.0	0.03	3.0	20.2 ± 8.2	14.0 ± 0.5	356.1	28.16	31.32	1.21	
2154−2105	0.571	17.6	0.03	2.6	19.4 ± 7.7	15.4 ± 0.5	380.7	26.93	30.58	1.40	
2158−1855	0.680	17.6	0.06	2.9	31.4 ± 8.5	15.6 ± 0.5	426.6	27.31	30.74	1.32	
2203−2134	0.575	18.2	0.05	2.4	35.1 ± 8.9	15.2 ± 0.5	430.1	27.27	30.35	1.18	RL[a]
2207−1703	0.360	18.4	0.07	2.7	24.7 ± 8.6	19.0 ± 0.6	470.6	26.50	29.87	1.29	
2212−1759	2.210	17.9	0.04	2.3	23.0 ± 8.7	20.9 ± 0.6	466.6	28.28	31.61	1.28	RQ, BAL
2350−0132	0.995	17.4	0.07	3.4	22.7 ± 8.1	18.5 ± 0.6	587.6	27.49	31.15	1.41	
2353−0153	0.671	16.7	0.05	3.5	63.4 ± 12.5	19.1 ± 0.6	536.8	27.57	31.08	1.35	
2354+0048	0.987	18.5	0.06	3.0	19.6 ± 8.1	18.8 ± 0.6	595.3	27.36	30.70	1.28	

NOTE.—Table 1 is published in its entirety in computer-readable form in the AAS CO-ROM Series, Vol. 5.
[a] Radio data from Molonglo Reference Catalog (Large et al. 1981) or from Condon et al. 1994.

Hz^{-1}, (10) logarithm of the optical luminosity in units ergs s^{-1} Hz^{-1}, (11) the slope α_{ox} of a hypothetical power law connecting 2500 Å and 2 keV, (12) notes, including class designations. For radio loudness, we note RL, RQ, or RA, where RA means ambiguous (when a radio flux upper limit is consistent with either a radio-loud or a radio-quiet designation, see § 5). QSOs with clear broad absorption lines (§ 6) are noted as BAL, and strong Fe II QSOs (see § 7) are noted as Fe.

4. OPTICAL TO X-RAY POWER-LAW SLOPES

The best-fit linear regression of log l_x versus log l_{opt} yields an apparent power-law relationship between X-ray and optical luminosities that has been well studied in the past, particularly using data from the *Einstein* satellite (e.g., Zamorani et al. 1981; Tananbaum et al. 1986; Wilkes et al. 1994). Similar correlations have been demonstrated in other wavebands (e.g., Kriss 1988; Green, Anderson, & Ward 1992). Brinkmann, Siebert, & Boller (1994) have performed a *ROSAT* study of a heterogeneous sample of cataloged QSOs detected in both the RASS and Molonglo Reference Catalog of radio sources (Large et al. 1981). The current study is the first analysis of the optical to X-ray properties of a large optically selected sample using data from the *ROSAT* satellite.

The slope of a hypothetical power law connecting 2500 Å and 2 keV is defined as $\alpha_{ox} = 0.384 \log (l_{opt}/l_x)$, so that α_{ox} is larger for objects with stronger optical emission relative to X-ray. Figure 2*a* shows the a_{ox} histogram for the LBQS/RASS sample, which we contrast to two very different samples of X-ray–observed QSOs. The open histograms depict the entire sample including nondetections, which are *lower* limits to α_{ox}. Shaded regions represent detections only. All samples have been restricted to log $l_{opt} > 29.5$ for comparison to the LBQS. We thus cull 345 QSOs from the *Einstein Observatory* Extended Medium Sensitivity Survey (EMSS) sample (Fig. 2*c*; Stocke et al. 1991), a substantially complete X-ray–selected sample starting from optically identified, serendipitous X-ray sources in *Einstein* pointed IPC observations. We include 460 QSOs from the sample of Wilkes et al. (1994), a heterogeneous compilation of optically and radio-selected QSOs that were targets of *Einstein* IPC pointings (Fig. 2*b*). Exposure times of pointed observations are longer than RASS exposures by factors of 4–60. Thus, about 60% of the Wilkes et al. sample is detected, and flux sensitivities range as low as $\approx 1 \times 10^{-14}$ ergs cm^{-2} s^{-1}.

The probability that the LBQS/RASS distribution of α_{ox} is drawn from the same parent population as those of either the EMSS or Wilkes et al. samples is less than 0.01%, as determined by a Kaplan-Meier two-sample test that incorporates limits (Feigelson & Nelson 1985). However, the same test shows that the EMSS and Wilkes et al. distributions of α_{ox} are consistent with each other. The survivor functions (the Kaplan-Meier estimate of the cumulative number of objects with α_{ox} histograms for the two comparison samples extend to values near 2.0, including objects with very weak X-ray emission not detected in the RASS.

Figure 3 shows log l_{opt} versus log l_x for the LBQS/RASS sample. To study only detections excludes information from 90% of the LBQS/RASS QSOs, comprising nearly half the total X-ray source counts from the ensemble of 908 LBQS/QSOs. On the other hand (as discussed in § A1), the large

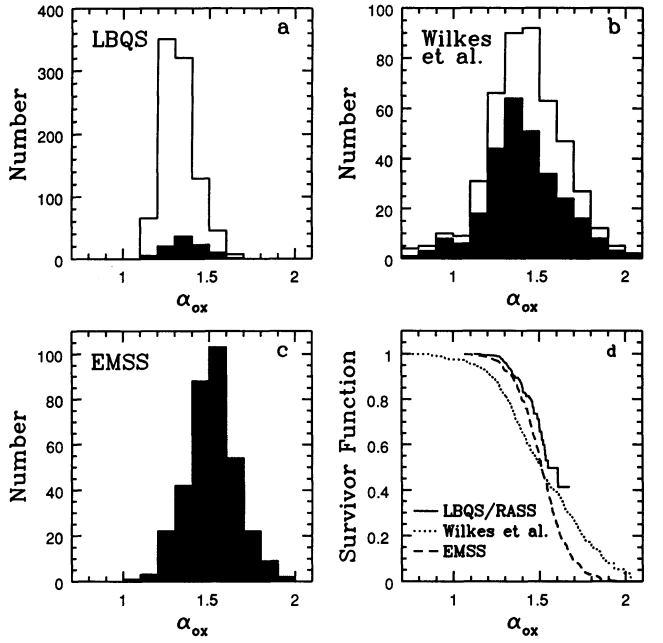

FIG. 2.—X-ray to optical spectral slope for three large QSO samples. Shaded histograms of α_{ox} represent X-ray detections, while open histograms depict the entire sample, including nondetections, which are *lower* limits to α_{ox}. All samples have been restricted to log $l_{opt} > 29.5$ for comparison to the LBQS sample, shown in (*a*). Although both the 460 QSO subsample of Wilkes et al. (1994) in (*b*) and the Stocke et al. (1991) EMSS subsample of 345 QSOs in (*c*) are taken from *Einstein* IPC pointings, the former is optically selected, and the latter is X-ray selected. Survivor functions [$P(>\alpha_{ox})$] for all three samples are contrasted in (*d*). The distribution of α_{ox} values for the 908 QSOs in the LBQS/RASS sample is significantly different from that of either of the pointed samples, while the EMSS and Wilkes et al. distributions are consistent with each other.

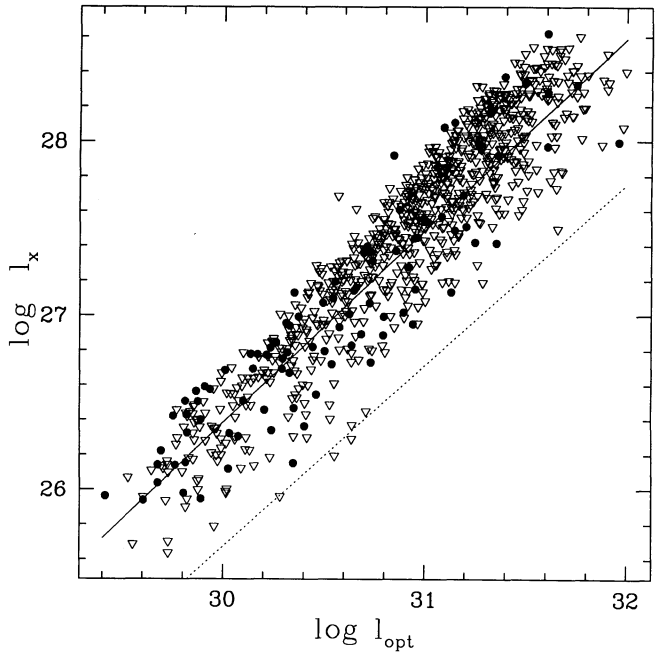

FIG. 3.—X-ray vs. optical luminosity for the LBQS/RASS sample. The 92 LBQS detections are shown as filled circles with their least-squares mean regression fit (*upper solid line*). Since 90% of the LBQS/RASS QSOs have only X-ray upper limits (*open triangles*), a fit using only detections is probably unreliable. The mean ASURV 2KM regression (*dotted line*) enables us to include upper limits. However, since only a small fraction of QSOs are detected, the 2KM regression is well below all the points and is also not reliable. This illustrates the need for stacking the LBQS/RASS QSO sample.

fraction of upper limits to l_x renders the survival analysis (ASURV) regressions unreliable. By stacking the X-ray data (discussed in detail in § A2), we effectively increase the sensitivity of the X-ray observations and include information from all QSOs regardless of detections status. For instance, only one individual QSO is detected with $\alpha_{ox} \approx 1.7$, whereas stacking allows us to study some properties of an *average* QSO with this continuum energy slope. Figure 4 shows the result of stacking LBQS QSOs in five bins each of Galactic column density N_H and optical luminosity log l_{opt}. All but two of the 25 bins are detections by our criteria, illustrating the power of the stacking technique. We use GaussFit (Jefferys et al. 1988a, b) for weighted orthogonal regression (hereafter WOR) of the stacked points (see § A3) and find a relationship between X-ray and optical luminosity (Fig. 4*a*) such that

$$\log l_x = 0.86(\pm 0.06) \log l_{opt} + 0.5(\pm 1.9) .$$

This nonunitary slope is highlighted by a correlation of α_{ox} with log luminosity, seen in Figure 4*b* for optical and Figure 4*c* for X-ray luminosity. The best-fit WOR for α_{ox} with optical luminosity yields

$$\alpha_{ox} = 0.08(\pm 0.02) \log l_{opt} - 1.0(\pm 0.7) .$$

To examine the effect of our choice of bins on these results, we compare WOR fits to $\alpha_{ox}(l_{opt})$ using several very different binnings in Table 2. Most fit results are consistent within less than 1.5 σ. A variety of reasonable spectral assumptions for α_o

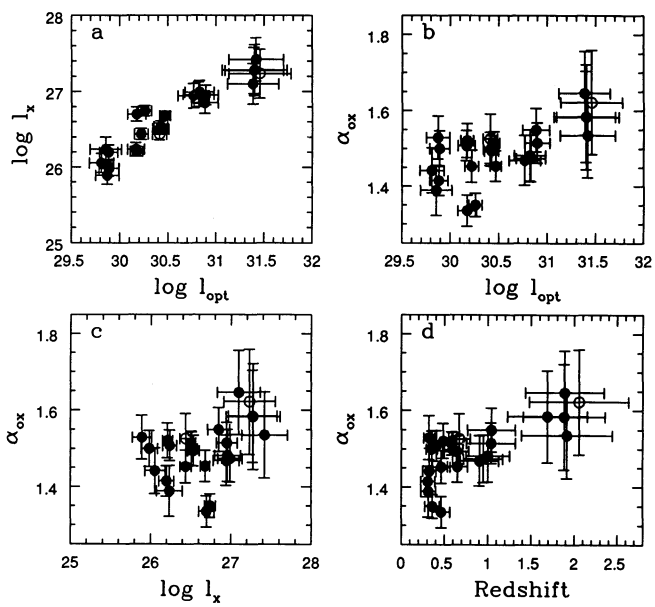

FIG. 4.—Continuum luminosities and spectral slopes for stacked QSO samples. Results of stacking LBQS/RASS QSOs in five bins each of Galactic column density N_H (bin edges are 1.0, 1.75, 2.25, 3.0, 3.25, and 6.0 × 10^{20} cm^{-2}) and rest frame 2500 Å luminosity log l_{opt} (bin edges are 29, 30, 30.25, 30.5, 31, and 32 ergs s^{-1} Hz^{-1}). All but two of the 25 bins are detections by our criteria. The usual strong correlations of (monochromatic rest frame 2 keV) X-ray luminosity with optical luminosity is seen in (*a*), with slope 0.86 (±0.06) between the log-luminosities, using a weighted orthogonal regression. The decrease in X-ray relative to optical emission with increasing luminosity (or redshift) is illustrated by the trends in α_{ox} with (*b*) log l_{opt}, (*c*) log l_x, and (*d*) redshift. Error bars represent dispersions.

TABLE 2

WOR REGRESSIONS OF $\alpha_{ox}(\log l_{opt})$

Bin Parameters	No. of Bins	Slope	Intercept
	Full LBQS/RASS Sample		
N_H/log l_{opt}	1/ 20	0.09±0.02	−1.4±0.7
N_H/log l_{opt}	6/ 7	0.07±0.02	−0.6±0.5
N_H/log l_{opt}	5/ 5	0.08±0.02	−1.0±0.7
N_H/log l_{opt}	1/ 5	0.11±0.03	−1.9±0.9
N_H/Redshift	1/ 17	0.11±0.01	−2.0±0.4
N_H/Redshift	5/ 5	0.11±0.02	−2.0±0.7
N_H/Redshift	1/ 4	0.15±0.01	−3.0±0.2
	Radio Quiet Sample		
N_H/Redshift	1/ 4	0.15±0.07	−3.1±2.3
	Radio Loud Sample		
N_H/Redshift	1/ 4	0.00±0.26	1.4±8.1

and Γ all lead to nonlinear slopes for the log l_x(log l_{opt}) relation. Boyle et al. (1993) derived a nearly identical slope (0.88 ± 0.08) for the log l_x(log l_{opt}) relation from a sample combining 42 QSOs X-ray–selected in deep *ROSAT* exposures with the EMSS sample. Similar slopes have been published in many earlier studies (e.g., Wilkes et al. 1994) using survival analysis on the fluxes of optically selected QSOs that were also *Einstein* targets. Margon et al. (1992) stacked the X-ray *images* of 146 LBQS QSOs serendipitously observed by *Einstein*. We note that for the binning in Table 2 most similar to that of Margon et al. (1992) we derive the identical slope and intercept.

Figure 4*d* demonstrates that α_{ox} also correlates with redshift, with a similar slope. Using bivariate Spearman rank tests (as implemented in ASURV; see § A1) on stacked points, we find that correlations of α_{ox} with either of log l_{opt} or redshift are significant at greater than 99.7% confidence for these data. Partial Spearman Rank Analysis (hereafter PSRA; Kendall & Stuart 1976) allows for the more general multivariate case, using a matrix of bivariate Spearman rank statistics as input. PSRA tests for correlations between subsamples of the matrix parameters while holding constant all other variables in the matrix. We find that the strength of correlations between any pair of α_{ox} and log l_{opt}, log l_x, and redshift are significant at greater than 99.5%. This result is not surprising: since the majority of QSOs in the magnitude-limited LBQS sample have apparent magnitudes near the plate limit, a strong correlation between redshift and optical luminosity exists. Thus, we cannot determine whether α_{ox} depends more strongly on luminosity or redshift. However, using different samples, Avni & Tananbaum (1986), Wilkes et al. (1994), and others have found that α_{ox} depends primarily on log l_{opt}. Most of our discussion will thus focus on this latter dependence.

The observed slope of an α_{ox}(log l_{opt}) relation may depend on a number of factors: (1) both the intrinsic and assumed spectral slopes in the optical and X-ray regimes, (2) the luminosity function and evolution in each of these bandpasses, and (3) a variety of selection effects and biases. The last point has been highlighted recently by Franceschini et al. (1994), who find slopes of the $l_x(l_{opt})$ relation consistent with linearity using an X-ray bright subset of the EMSS (Maccacaro et al. 1991) plus the deep *ROSAT* survey of Boyle et al. (1993).

An important final check on our stacking technique is to run exactly these same tests on our control sample. We have appended the X-ray control data to the actual LBQS optical data used above. The results, using the same bins, are shown in Figure 5. All points are limits, except for a single detection that is barely realized [at $4.08(C^s_{bkg})^{1/2}$] in one of the 25 bins. The only significant correlation, between log l_{opt} and upper limits to log l_x (Fig. 5*a*), is expected, since these luminosities have been multiplied by the identical redshift factor.

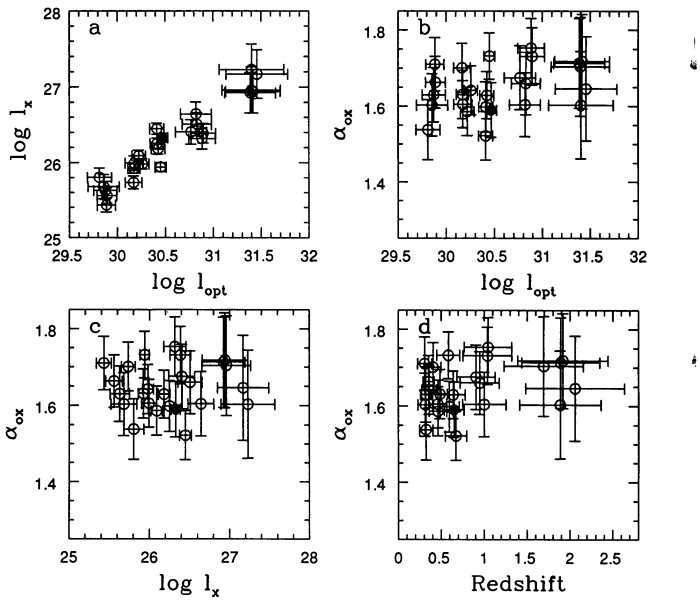

FIG. 5.—Continuum luminosities and spectral slopes for a stacked control sample. To check our stacking technique, we repeat the same procedure that generated the previous figure, this time using our control sample. A marginal detection (*filled circle*) occurs in one of the 25 bins. The apparent correlation between l_{opt} and upper limits to l_x in (*a*) is expected, since both have been multiplied by the identical redshift factor.

5. RADIO-QUIET VERSUS RADIO-LOUD

Optically selected samples of QSOs appear to be separated into two distinct populations, radio-loud (RL) and radio-quiet (RQ; e.g., Kellerman et al. 1989). It is now accepted that for a given optical luminosity, the average X-ray luminosity of RL QSOs is higher than that of RQ QSOs (e.g., Zamorani et al. 1981, Avni & Tananbaum 1986; Worrall et al. 1987). Furthermore, power-law fits to the X-ray spectrum of RL QSOs are characterized by flatter slopes (e.g., Wilkes & Elvis 1987; Lawson et al. 1992; Shastri et al. 1993). The *ROSAT* X-ray properties of radio-loud QSOs have been studied by Brinkmann et al. (1994) and Brunner et al. (1992) using the Molonglo (Large et al. 1991) and Kühr et al. (1979) surveys, respectively.

The radio properties of LBQS QSOs have been investigated using VLA observations at 8.4 GHz sensitive to about 0.25 mJy (the 3 σ) noise limit; Visnovsky et al. 1992, Hooper et al. 1995). This VLA sample was selected to cover the brightest $\approx\frac{1}{4}$ of the QSOs over the full redshift range of the LBQS. We also include 26 (much less sensitive) detections from the sky surveys of Condon et al. (1994) (5 GHz) or Large et al. (1981) (408 MHz). In sum, radio data are currently available for 237 QSOs that also have high-quality RASS data. We convert all radio fluxes to 8.4 GHz by assuming a radio spectral slope of −0.5. For purposes of comparison, we define an object as radio-loud if the log ratio of the emitted monochromatic luminosities at 8.4 GHz and 4410 Å, log $R \equiv \log (l_{8.4\ \mathrm{GHz}}/l_{4410\ \text{Å}})$, is

greater than unity. In the current sample, this ratio ranges from (an upper limit of) -0.70 to 4.54, with a mean of -0.06 from survival analysis. A different definition of radio loudness, which divides QSOs into two populations at an 8.4 GHz radio luminosity of about 10^{25} W Hz^{-1}, would redefine two more QSOs as radio-loud and does not substantially affect any of the results we present here.

Included in our QSO subsamples defined by radio loudness are only those QSOs with radio detections or limits that categorize them unambiguously as RL or RQ QSOs. There is only one RL QSO below $z = 0.4$, compared with 20 RQ QSOs. Furthermore, $z = 0.4$ corresponds to the mean redshift of QSOs with $M_B = -24$: Hooper et al. (1995) and Della Ceca et al. (1994) find that the fraction of RL QSOs decreases abruptly for absolute magnitudes fainter than this. There is also only one RL QSO above $z = 2.4$, compared to 26 RQ QSOs. For these reasons, to enable a fair comparison between the RL and RQ QSO samples, we restrict the redshift range of both samples to $0.4 < z < 2.4$. This leaves 40 RL QSOs ($\bar{z} = 1.2 \pm 0.5$) and 147 RQ QSOs ($\bar{z} = 1.6 \pm 0.6$).

Of RQ QSOs, 16 (11%) are detected in the RASS, compared to 10 RL QSOs (25%). We can compare count rates in RL and RQ QSO samples independent of assumed spectral models or detection thresholds via stacking. For convenient comparison, we quote average RASS count rates normalized to counts (per QSO) using a typical RASS exposure time of 600 s. The mean number of counts from stacking is 12.9 ± 1.2 s^{-1} for RL QSOs, significantly higher than the 8.0 ± 0.6 counts we find for RQ QSOs. Since all the RQ QSOs are from the somewhat optically brighter VLA-observed subsample (as compared to less than half the RL QSOs), the intrinsic difference may be even stronger. However, the observed difference here is nearly compensated for by the difference in mean redshifts between the RL and RQ subsamples.

As usual, to derive X-ray fluxes and luminosities requires the assumption of an X-ray spectral slope. Unlike most previous studies, we have mean *ROSAT* spectral slopes available from these identical samples and data (Schartel et al. 1995). We thus assign spectral slopes $\Gamma = 2.1$ to RL, and $\Gamma = 2.7$ to RQ QSOs. From stacking all QSOs in the RL and RQ subsamples, we find overall means (with their dispersions) for $\log l_x$ of 27.45 ± 0.04 and 27.19 ± 0.03, so that RL QSOs appear to be about twice as luminous in X-rays. For mean α_{ox} values, we find 1.44 ± 0.13 for RL and 1.57 ± 0.15 for RQ QSOs. The optical-to-X-ray properties of these 40 RL and 147 RQ QSOs are compared in Figure 6. We stacked RL and RQ QSOs separately in bins of redshift (bin edges are 0.4, 0.6, 1, 1.4, and 2.4). Although the number of RL QSOs in these bins is small (3, 11, 14, and 12, respectively), we note consistently larger α_{ox} for RQ QSOs. In the highest redshift bin ($\bar{z} \approx 1.9$), RL QSOs are significantly more luminous in X-rays, by a factor of about 5. This is in qualitative agreement with a variety of previous *Einstein* studies (e.g., Bechtold et al. 1994; Wilkes et al. 1994; Worrall et al. 1987; Zamorani et al. 1981).

The trends in luminosity in Figures 6*a* and 6*c* suggest that α_{ox} may be approximately constant in RL QSOs, i.e., these objects maintain a nearly linear relationship between l_{opt} and l_x. This is quantified by the Gaussfit WOR listed in Table 2 for RL QSOs, which is consistent with no trend of α_{ox} with l_{opt}. In RQ QSOs, on the other hand, l_x appears to increase more slowly than l_{opt}, so that α_{ox} increases with l_{opt}. Since the slope of the $\alpha_{ox}(l_{opt})$ relation for RQ QSOs appears to be similar to that of the LBQS/RASS sample as a whole (see Table 2), the increase in α_{ox} with luminosity found for the overall LBQS/RASS sample may be attributable to the contribution of the 9/10 of QSOs that are radio-quiet. However, it is clear from Table 2 that the formal difference in slope between RL and RQ subsamples is not significant, probably due to the small number of known RL QSOs. Wilkes et al. also found the slopes of an assumed $\alpha_{ox}(\log l_{opt})$ relation to be consistent for their RL and RQ subsamples. Based on a very small sample of high-redshift PSPC pointings, Bechtold et al. (1994) and Pickering, Impey, & Foltz (1994) similarly find evidence for an upward trend in α_{ox} with luminosity in RQ QSOs, but *not* in RL QSOs, as seen in Figure 6*b*.

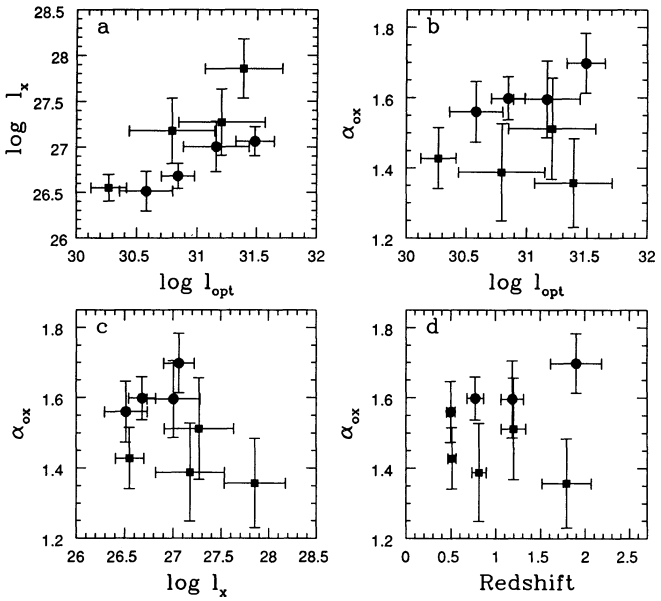

FIG. 6.—Continuum luminosities and spectral slopes for radio-loud (RL) vs. radio-quiet (RQ) QSOs. The optical-to-X-ray properties of the 41 RL and 193 RQ QSOs are compared by stacking RL QSOs (*filled circles*) and RQ QSOs (*filled squares*) separately in bins of redshift (bin edges are 0.4, 0.6, 1, 1.4, and 2.4; this excludes only two RL QSOs). Although the number of RL QSOs in these bins is small (3, 11, 14, and 12, respectively), we note significant differences between RL and RQ QSO samples that appear to become more pronounced as redshift (or optical luminosity) increases.

The mean α_{ox} values we find above appear to differ by less than 1 σ between RQ and RL QSOs. This result may be less dramatic than previous work for a variety of reasons: (1) our conservative use of dispersion rather than the error in the mean (see § A2 below), (2) our attempt to match redshift distributions, (3) our use of the correct X-ray spectral slopes and homogeneous X-ray data. Selection bias in the radio observations might also affect our result. The most rigorous comparison between RL and RQ QSOs would exclude those (RL) QSOs found by correlation with the non-VLA surveys. However, their exclusion does not significantly change our results and would in any case significantly decrease the RL sample size. The apparent increase with l_{opt} in the separation of α_{ox} between RL and RQ QSOs evident in our Figure 6 warrants further investigation to clarify the strength and cause of the observed trend.

6. BAL VERSUS NON-BAL QSOs

About 10%–15% of optically selected QSOs have optical/UV spectra that show deep absorption troughs displaced blueward from the corresponding emission lines is the high

ionization transitions of C IV, Si IV, N V, and O IV. Years after the discovery of broad absorption line (BAL) QSOs, the geometry, covering factor, temperature, density, metallicity, and ionization parameter of the absorbing clouds are still poorly understood. Since BAL spectra in the UV are often partly saturated and may contain unresolved components, the properties of BAL clouds are not well constrained by optical/UV data alone. Techniques have recently been developed by Mathur (1994) and Mathur et al. (1994) that simultaneously exploit UV and X-ray spectra to constrain the allowed ranges of the parameters just listed. An application of these techniques to BAL QSOs may eventually provide stronger constraints on BAL clouds, but to date the X-ray properties of BAL QSOs as a class are only poorly understood, partly for lack of a homogeneous sample with available X-ray data.

Our BAL QSO subsample includes only those with clear BALs in their optical spectra, and we conservatively exclude several QSOs with ambiguous BAL classifications, resulting in a subsample of 37 BAL QSOs (each noted accordingly in Table 1). The broad absorption lines just blueward of C IV that are minimally required for a BAL QSO classification here cannot be detected in the optical below $z \approx 1.3$. Therefore, to enable a fair comparison to our BAL QSO subsample ($\bar{z} = 1.9$), we truncate the non-BAL sample below redshift 1.3, leaving 36 BAL and 363 non-BAL QSOs with high-quality RASS data. Once this is done, no significant differences are seen in the distributions of redshift, B_J magnitude, Galactic N_H, or RASS exposure time between the BAL and non-BAL samples.

Only one BAL QSO in the LBQS/RASS sample is detected in the RASS, so that we cannot perform extensive X-ray analysis of this subsample. However, we can again examine the average X-ray properties of BAL QSOs by stacking, and by comparing BAL QSO properties with similar stacked non-BAL samples. One such measure is provided by comparing the number of net stacked counts of BAL and non-BAL subsamples (normalized to a 600 s exposure). For the stacked 36 BAL QSOs, this value is -0.15 ± 1.1, compared to 3.2 ± 0.4 for stacking the subsample of all 363 non-BAL QSOs. Our conservative upper limit of $4(C^s_{bkg})^{1/2}$ to the stacked counts for the 36 BAL QSOs yields the following limits assuming $\Gamma = 2.5$: $\log l_x \leq 27.3$, and $\alpha_{ox} \geq 1.6$, where $\log \overline{l_{opt}} = 31.4$ for the subsample. At the 4 σ level, the X-ray properties of BAL QSOs are marginally consistent with those of the ensemble of LBQS/RASS QSOs as displayed in Figure 4. However, these limits are also fully consistent with the above 2–3 σ suggestion that BAL QSOs are underluminous or strongly absorbed in X-rays. At the very least, these final conservative limits show that BAL QSOs as a class are definitively *not* X-ray–loud. A more consistent comparison of $\log l_{opt}$ and α_{ox} values is obtained if the B_J magnitudes for BAL QSOs are corrected for the presence of the absorption lines. The "BAL K-correction" (Stocke et al. 1992) for $z \approx 2$ QSOs is 0.15 ± 0.08. Application of this correction to the mean BAL mag yields results identical to within the errors.

In a second approach using a Monte Carlo simulation, we randomly picked 1000 subsamples of 36 non-BAL QSOs each from the same list of 363 non-BALs and stacked their X-ray data as with the 36 actual BAL QSOs. Only five in 1000 trials stacking non-BAL subsamples achieve low net count rates than for the BAL QSO subsample (Fig. 7). Since BAL QSOs may be a subgroup of the class of RQ QSOs (Stocke et al. 1992), we also compared the BAL subsample to the sample of 94 non-BAL QSOs with $z > 1.3$ that are known to be radio-

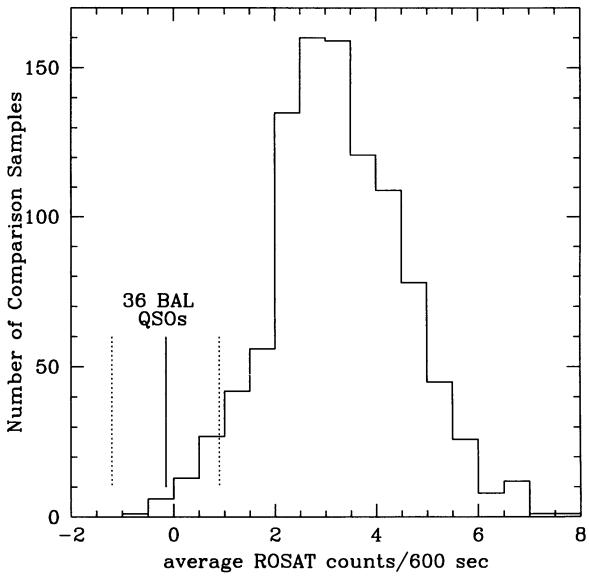

FIG. 7.—Monte Carlo simulations for BAL QSOs. We stacked 1000 random subsamples of 36 QSOs from a list of 363 definite ($z > 1.3$) non-BAL QSOs, for comparison to the true BAL sample of 36 QSOs. Counts are normalized to a RASS exposure time of 600 s. The number of stacked counts for the BAL sample is indicated, with errors (square root of the area-normalized background counts) shown as dotted lines to either side. Comparison to the histogram of stacked counts for the 1000 comparison samples reveals that only five in 1000 trials generates equal or fewer counts. The sample of 36 stacked BAL QSOs thus appears to be relatively X-ray quiet.

quiet. From this (somewhat brighter B mag) comparison sample, we *never* achieved lower count rates in 1000 trials. Both the above approaches suggest (at 2–3 σ) that BAL QSOs *as a class* are underluminous in X-rays compared with non-BAL QSOs.

Since *ROSAT* count rates for QSOs at similar redshift depend on more than bolometric luminosity, we now consider the possible effects of X-ray spectral properties or Galactic absorption on our result. The mean Galactic N_H is about 2.7×10^{20} cm^{-2} for both BAL and non-BAL samples. If these represent total line-of-sight hydrogen column densities, then BAL X-ray spectral slopes would need to be unreasonably soft ($\Gamma \gg 3$) to account for the difference in observed counts. This leaves strong absorption intrinsic to the BALs as the most likely culprit, a result not incongruous with the strong UV absorption that leads to their BAL classification. Further analysis of the absorbers in BAL QSOs would benefit from the treatment recently applied to the X-ray/UV absorbing outflows in 3C 351 and 3C 212 (Mathur et al. 1994; Mathur 1994). However, one deterrent to such analysis has been the dearth of BAL QSOs at typical BAL discovery redshifts with sufficiently strong X-ray emission to permit X-ray spectral analysis from exposures of reasonable length.

The only BAL QSO detected in X-rays in the LBQS/RASS sample is 2212−1759. Given its large redshift of 2.21, and our result that BAL QSOs are likely to be X-ray–quiet, this detected BAL seems worthy of further study. However, since we have estimated a spurious detection rate of $\lesssim 5\%$ from the control sample (§ 3), we expect at most one or two BAL QSOs to be incorrectly identified as a RASS detection. Examination of the LBQS plates reveal several other possible sources of X-ray emission. One nearby object is a $B_J = 14.0$ star about 50″ SE of the BAL QSO position. Conservatively using

$V = 14.5$ and the observed RASS flux, we find $\log f_x/f_V < -0.9$, consistent with ratios observed for stars of mid-M type or later (Stocke et al. 1992). However, our optical spectrum of the object (taken with the MMT Blue Channel spectrograph on 1994 June 1) shows the star to be of type K2 or earlier, with no emission lines that might indicate chromospheric activity, thus making the star an unlikely X-ray source. Another stellar object 32″ from the QSO is (judging by the LBQS plate prism spectrum) a late K or M star, but with $B_J = 18.4$ it could not produce the observed X-ray flux. A ($B_J \approx 19.5$) galaxy 47″ from the BAL QSO is also not likely to be the RASS source given the f_x/f_V ratios typical of galaxies. We thus believe the BAL 2217−1759 to be the source of the X-rays we have detected in the RASS, and so a good candidate for X-ray spectral analysis.

7. Fe II VERSUS NON-Fe II

There is some evidence that QSOs with strong Fe II emission may have different X-ray properties than otherwise similar QSOs showing weak or nonexistent Fe II. Using a heterogeneous sample of 18 objects ($\bar{z} = 0.15$), Shastri et al. (1993) found that (radio-quiet) QSOs with strong optical Fe II emission show softer (steeper) *Einstein* spectral slopes. In a heterogeneous sample of 55 QSOs ($z < 0.5$, ≈30% radio loud), Corbin (1993) found a strong anticorrelation between the optical Fe II/Hβ ratio and *Einstein* X-ray luminosity, as well as a weaker anti-correlation with EW Fe II (all these Fe II measures used the iron complex near λ4570). Their results suggest that Fe II QSOs may be underluminous in X-rays. However, the physical significance of these correlations has been challenged on the grounds of incompleteness, differences in sample sizes, and different techniques used to measure the strength of the iron complexes (e.g., Boroson & Green 1992; Zheng & O'Brien 1990). We attempt to clarify these issues here with a small but homogeneous sample.

From previous LBQS discovery papers (Morris et al. 1991, and references therein), 22 QSOs were flagged as having strong UV Fe II emission. Seven more QSOs from Paper II of the series (Foltz et al. 1989) were classified as possessing strong Fe II but were not flagged in that paper: 0010+0146, 0020−0300, 2237−0234, 2245−0055, 2249+0234, 2356+0207, and 2358−0246. Although the Fe II flag represents a subjective judgment, these QSOs are likely to be among those with the strongest iron emission in the LBQS sample. Of the total of 29 Fe II QSOs, 23 have high-quality RASS data (all flagged in Table 1). Of 12 Fe II QSOs with radio data, nine are radio-quiet; 0103−2753 is a BAL QSO, while 1148−0033 and 0107−0235 are radio-loud QSOs. The latter only is detected in the RASS.

The redshift range most likely to lead to an Fe II classification is $0.4 \leq z \leq 1.5$, due to the iron feature under [Ne IV] λ2423. We thus restrict the redshifts of both the Fe II and the comparison non–Fe II sample to within this range. This excludes one Fe II QSO, 2249+0234, with $z = 0.29$. The mean redshift for the sample of 22 Fe II QSOs in the LBQS/RASS is 0.88. The comparison sample of 467 non–Fe II QSOs has a mean redshift of 0.96. We find a mean B_J magnitude about 0.4 mag brighter for the Fe II sample, but since some of this small difference is due to the iron emission itself, we do not attempt further restictions to more closely match the sample distributions. Of the 22 Fe II QSOs, seven are detected in the RASS. This represents 3 times the overall detection rate in the non–Fe II sample. The mean α_{ox} for the Fe II sample (1.5 ± 0.1) is not significantly different from that of the non–Fe II QSOs (1.6 ± 0.3). However, use of a continuum optical magnitude with the effects of the Fe II emission removed is probably more consistent, and would further decrease the derived α_{ox} for Fe II QSOs.

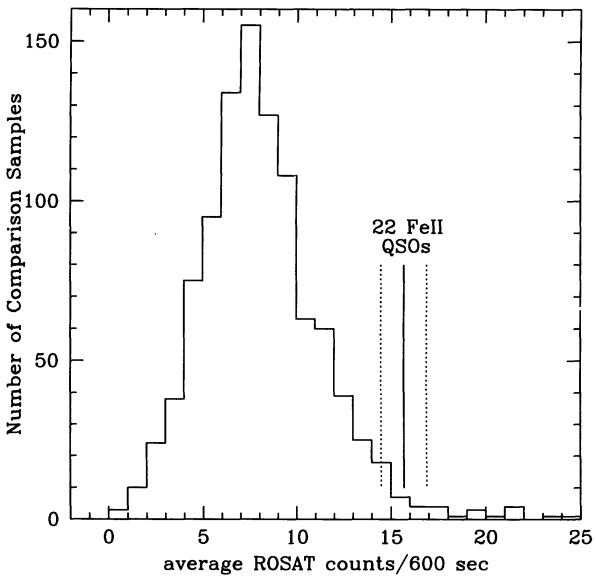

FIG. 8.—Monte Carlo simulations for Fe II-strong QSOs. We stacked 1000 random subsamples of 22 QSOs from a list of 474 ($0.4 \leq z \leq 1.5$) QSOs showing no strong Fe II emission, for comparison to the true Fe II strong sample of 22 QSOs. Counts are normalized to a RASS exposure time of 600 s. The number of stacked counts for Fe II QSOs is indicated, with errors (square root of the area-normalized background counts) shown as dotted lines to either side. Since the probability of obtaining this same number of counts or larger is less than 2%, the sample of 22 stacked Fe II QSOs appears to be X-ray bright.

The mean number of counts from stacking the 22 QSOs in the Fe II–strong sample is thus 14.0 ± 1.7 (again quoting RASS counts normalized to a 600 s exposure). A greater number of counts is achieved for only 2.2% of 1000 subsamples of 22 QSOs randomly selected from the non–Fe II sample (Fig. 8). The mean count rate of these non–Fe II subsamples is 7.8 ± 2.6, nearly a factor of 2 lower. It thus appears that QSOs with strong UV Fe II emission may be unusually strong X-ray emitters.

We now consider the possible effects of X-ray spectral properties or Galactic absorption on this result. The mean Galactic absorption $\bar{N}_H$ is virtually identical for the two subsamples ($N_H \approx 2.7 \times 10^{20}$ cm^{-2}). Schartel et al. (1995) find for this same Fe II subsample a photon index $\Gamma = 2.8 \pm 0.2$, which is consistent with the value $\Gamma = 2.7 \pm 0.1$ they derive for the non–Fe II subsample. With a line-of-sight hydrogen column density ($N_H \approx 2.7 \times 10^{20}$ cm^{-2}), if differing X-ray spectral slopes are to explain a factor of 2 difference in count rates, we would need to assume values of $\Gamma < 2.2$ for the Fe II QSOs and $\Gamma > 3.0$ for the non–Fe II QSOs. The sense of such a trend is in contradiction to the results of Shastri et al. (1993) mentioned above, albeit for a very different sample. More importantly, these spectral indices are 3 σ in opposite senses from the values measured for their respective samples (Schartel et al. 1995). Therefore, we believe that a difference in X-ray spectral index can be ruled out as the sole cause of the observed difference in X-ray counts.

According to the models of Krolik & Kallman (1988), the continuum source responsible for creating rest frame optical Fe II lines comes almost entirely from X-rays above about 1 keV. Data from the small, heterogeneous sample of Shastri et al. (1993) suggested instead that QSOs with stronger optical Fe II had, if anything, *softer* X-ray spectral slopes. The rest frame UV Fe II multiplets we study here, according to the model, originate at lower optical depths where soft X-ray and EUV photons contribute to the heating. Our finding that LBQS QSOs with strong UV Fe II are relatively bright in the *ROSAT* soft X-ray bandpass is consistent with this model. On the other hand, Schartel et al. (1995) find no significant differences in X-ray spectral slopes between the LBQS Fe II–strong and comparison subsamples. Stronger tests of the model would be obtained for QSOs with both optical and UV Fe II measurements available for comparison to X-ray slopes and luminosities.

8. CONCLUSIONS

We detect 10% of the 908 LBQS QSOs observed in the RASS. The strong correlation between $l_{\rm opt}$ and l_x fits a nonlinear power law. This is reflected in a correlation between the optical-to-X-ray spectral slope α_{ox} and the rest-frame 2500 Å luminosity such that $\alpha_{ox} = 0.08(\pm 0.02) \log l_{\rm opt} - 1.0(\pm 0.7)$. This confirms, using a large, homogeneous sample, similar results found using independent techniques (e.g., Margon et al. 1992; Wilkes et al. 1994).

We offer the first published comparison of the *ROSAT* X-ray properties of well-defined subsamples and find only marginal mean differences in log l_x and α_{ox} for RQ QSOs compared to RL QSOs. However, differences in X-ray emission appear to increase as a function of redshift (or optical luminosity). The $l_x(l_{\rm opt})$ relation appears to be nearly linear for RL QSOs, while for RQ QSOs the X-ray luminosity may increase more slowly. This is equivalent to the statement that the $\alpha_{ox}(\log l_{\rm opt})$ relation is steeper for RQ QSOs. In an optically selected sample such as this, the often-observed increase of α_{ox} with $l_{\rm opt}$ could thus be attributable mostly to the contribution of the $\approx 90\%$ of the sample that is radio-quiet. Analysis of the strength and origin of these apparent trends will benefit from a larger number of radio observations of LBQS QSOs or from deeper X-ray observations.

We use stacking to compare a subsample of 36 BAL QSOs to a comparison sample of non-BAL QSOs in a similar redshift range. Even though one BAL is detected, the BAL subsample stacks to a *ROSAT* count rate of -0.0003 ± 0.002 s^{-1}. Conservative upper limits to l_x and α_{ox} for the BAL subsample are consistent with the properties of LBQS/RASS QSOs of similar $l_{\rm opt}$. However, Monte Carlo tests of random non-BAL subsamples result in similar count rates less than 1% of the time, suggesting that the BAL class is likely to be X-ray quiet. We suggest that a very soft intrinsic X-ray spectral slope, combined with Galactic absorption, is insufficient to account for the low X-ray counts from the BAL QSOs. This leaves strong absorption intrinsic to the BALs as the most likely culprit.

We contrast a subsample of 22 QSOs showing strong UV Fe II emission to a sample of QSOs in a similar redshift range. The stacked Fe II QSO subsample has a *ROSAT* count rate twice as high as the mean, which occurs $\approx 2\%$ of the time in Monte Carlo tests of our comparison sample. The Fe II multiplets we study here may be generated at lower optical depths where soft X-ray and EUV photons can contribute to the heating.

The *ROSAT* project is supported by the Bundesministerium für Forschung and Technologies (BMFT). We thank our colleagues from the *ROSAT* group for their support. This research was supported through NASA grant NAG5-1623. Support for P. J. G. was provided by the NSF through grant INT 9201412, and by NASA through grant HF-1032.01-92A awarded by the Space Telescope Science Institute, which is operated by the Association of Universities for Research in Astronomy, Inc., under NASA contract NAS5-26555. P. J. G. also wishes to thank the Institute of Astronomy and the MPE for their kind hospitality. N. R. S. acknowledges a Max Planck Fellowship, and C. B. F. acknowledges the support of NSF grant AST 9320715. We thank Silvano Molendi for helpful comments.

APPENDIX

STATISTICAL METHODS

Since only about 10% of LBQS QSOs are detected in X-rays, it is critical to include the information for QSOs that do not meet the detection criteria. We describe briefly our use here of two methods: stacking and survival analysis. Our most important results are derived rom stacking of the X-ray counts.

A1. SURVIVAL ANALYSIS

The widely distributed survival analysis package ASURV (Rev 1.1; LaValley, Isobe, & Feigelson 1992) implements the methods presented in Feigelson & Nelson (1985) for univariate problems and Isobe, Feigelson, & Nelson (1986) for bivariate problems. When no upper limits are present, all these tests reduce to the expected results from standard statistical analyses of distributions: means, two-sample tests, correlations, or regressions.

The particular ASURV techniques we use are the same as delineated in Green et al. (1992). The Kaplan-Meier nonparametric maximum-likelihood estimator includes either lower or upper limits to the data. This method works well with any variable whose censoring distribution is independent of the values themselves. This is clearly not a description of flux measurements in a flux-limited sample such as the RASS wherein all the censored values are found near the sensitivity threshold of the survey. The effects of nonrandom censoring are greatly decreased when using flux *ratios*.

For univariate two-sample comparisons, we require a probability $P < 0.02$ to consider two samples to be "significantly different." A similar criterion is applied to bivariate correlation analysis. The two-dimensional Kaplan-Meier test (Schmitt 1985, hereafter 2KM) permits linear regression with limits in either axis.

Although the median of a univariate distribution is always well defined, if the lowest (highest) point in the data set is an upper (lower) limit, the mean is not, since the distribution is not normalizable, so that the outlying censored point must be redefined as a detection. Although redefinition of a single limit as a detection may be acceptable for some univariate distributions, if only a small fraction of objects are detected, bivariate regressions may not converge or can yield misleading results, when many limits at bin edges need to be redefined as detections. The result is that the derived best-fit linear regression may fall below most points in a plot (e.g., of log l_{opt} vs. log l_x, see Fig. 3), and is quite sensitive to the adopted bin sizes. Results from survival analysis may thus depend strongly on the number of detections, and therefore on the detection threshold, since in a flux-limited sample, most detections are near that threshold (e.g., Anderson & Margon 1987). For these reasons, when raw data are available, our analysis relies strongly on stacking.

A2. X-RAY FLUX STACKING

Stacking makes unbiased use of the X-ray information from all objects, a feature that is ideally suited to a large sample with raw source and background counts available. Results from stacking are independent of the adopted X-ray detection threshold (see Anderson & Margon 1987). X-ray stacking has proven useful in a variety of astrophysical applications (e.g., Caillaut & Helfand 1985; Anderson & Margon 1987). Indeed, the technique was already used on a subsample of 146 LBQS QSOs serendipitously included in *Einstein* pointed observations (Margon et al. 1992).

In the current study, we use our raw RASS source counts in an analogous procedure to find the average X-ray flux for a selected subsample of QSOs. The raw RASS counts in the source and background apertures for each QSO are separately summed, as are their effective exposure times. The final, stacked QSO effectively has a much longer *ROSAT* exposure time and thus a much more sensitive X-ray observation. Errors in both source and background counts are correctly propagated in the stacking process. The detection threshold for a stacked QSO is defined identically to that for an individual QSO as outlined above. Bins are defined interactively to achieve detections without undue sacrifice of resolution in the binning parameters (e.g., l_{opt}, redshift, or N_H). Any results we quote are robust and have been reproduced with a variety of binnings.

Galactic hydrogen column density N_H determines X-ray counts-to-flux conversion factors (CFs). Therefore, when the number of QSOs in tested samples permits, we stack in bins of N_H so that the use of a mean CF causes no more than $\approx 20\%$ error in X-ray flux for QSOs within a bin (and thereby an error in α_{ox} of less than 0.03). The resulting l_x or α_{ox} values (whose spread within an l_{opt} bin may be seen e.g., in Fig. 4), show no correlation between N_H and either l_x or α_{ox} as expected, since (stacked) counts remain the primary determinant of l_x.

We calculate X-ray fluxes for stacked QSOs assuming an X-ray photon index Γ appropriate to the sample, as derived by Schartel et al. (1995). Errors for the stacked X-ray luminosities are derived from the errors in X-ray source counts σ_i of individual QSOs. If we represent the number of counts in a stacked image as S, with error σ_S, the X-ray luminosity is proportional to S, with the constant of proportionality k depending on (the mean values of) N_H and redshift, and on the assumed Γ. The uncertainty in the value of $\log l_x$ is independent of k and may be expressed simply as

$$\sigma = 0.5 \log \left(\frac{S + \sigma_S}{S - \sigma_S} \right).$$

Errors in optical luminosity or in redshift are taken to be the rms dispersion of these values among QSOs in a bin. Although the error in the mean values may be much lower, use of the dispersion automatically includes such effects as intrinsic dispersion in QSO properties, magnitude errors, and errors in extinction estimates. For any wave band, we calculate the log of the mean flux (rather than the mean of log) for QSOs in a stacking bin, so that the slope we derive between the 2500 Å and 2 keV is $\alpha_{ox}^{\rm eff} = 0.384 \log \langle l_{opt}/l_x \rangle$.

While only a modest fraction of the QSOs will be individually detected in X-rays, the entire RASS-observed sample of 908 QSOs is effectively utilized in these stacked X-ray fluxes, to obtain (in most cases) X-ray detections of the stacked QSO within each bin. Binning and stacking thus allow us to study the evolution of X-ray properties, and the relationship between X-ray and optical continuum luminosities. Novel stacking techniques have recently been developed that allow objects to be binned together retaining energy information for X-ray spectral analysis, even through a range of Galactic hydrogen column densities (Schartel et al. 1995). The spectral slopes derived for a given sample may then be used on stacked counts for these samples for calculation of mean fluxes and luminosities, as they are in the current work for the full LBQS/RASS sample, as well as the RL and RQ QSO subsamples.

A3. LINEAR REGRESSION

Unless the intrinsic physical relationships underlying correlations between observed parameters are known, the simplest and least biased estimator of the form of their interdependence should be used. The *simplest* relationship is linear and may be estimated by ordinary least-squares (OLS) regression when all points are detected. The *least biased* such line is found by weighted orthogonal regression (WOR), which makes no assumptions as to which variable is dependent. For stacked QSO data that has no (or an insignificant number of) limits, we apply weighted orthogonal regression using GaussFit (Jefferys et al. 1988a, b). GaussFit yields error estimates on the fit and can incorporate the general heteroscedastic case, where measurement errors are different for each point and in each variable.

REFERENCES

Anderson, S. F., & Margon, B. 1987, ApJ, 314, 111
Aschenbach, B. 1988, Appl. Opt., 27, 1404
Avni, Y., & Tananbaum, H. 1986, ApJ, 305, 83
Bade, N., Engels, D., Fink, H., Hagen, H.-J., Reimers, D., Voges, W., & Wisotzki, L. 1992, A&A, 254, L21
Bechtold, J., et al. 1994, AJ, 108, 374
Blair, M., & Gilmore, G. F. 1982, PASP, 94, 742
Boroson, T. A., & Green, R. V. 1992, ApJS, 80, 109
Boyle, B. J., Fong, R., Shanks, T., & Peterson, B. A. 1990, MNRAS, 243, 1
Boyle, B. J., Griffiths, R. E., Shanks, T., Stewart, G. C., & Georgantopolous, I. 1993, MNRAS, 260, 49
Brinkmann, W., Siebert, J., & Boller, T. 1994, A&A, 281, 355
Brunner, H., Friedrich, P., Zimmermann, H.-U., Staubert, R. 1992, in X-Ray Emission from AGN and the Cosmic X-Ray Background, ed. W. Brinkmann & J. Trümper (Garching: Max Planck), 198
Burstein, D., & Heiles, C. 1978, ApJ, 225, 40
———. 1982, AJ, 87, 1165
Caillaut, J.-P., & Helfand, D. J. 1985, ApJ, 289, 279
Chaffee, F. H., Foltz, C. B., Hewett, P. C., Weymann, R. J., Morris, S. L., Anderson, S. F., & MacAlpine, G. M. 1991, AJ, 102, 461
Condon, J. J., Broderick, J. J., Seielstad, G. A., Douglas, K., & Gregory, P. C. 1994, AJ, 107, 1829
Corbin, M. R. 1993, ApJ, 403, L9
Cristiani, S., & Vio, R. 1990, A&A, 227, 485
Della Ceca, R., Zamorani, G., Maccacaro, T., Wolter, A., Griffiths, R., Stocke, J. T., & Setti, G. 1994, ApJ, 430, 533
Feigelson, E. D., & Nelson, P. I. 1985, ApJ, 293, 192
Fisher, J. R., & Tully, R. B. 1981, ApJS, 47, 139
Foltz, C. B., Chaffee, F. H., Hewett, P. C., MacAlpine, G. M., Turnshek, D. A., Weymann, R. J., & Anderson, S. F. 1987, AJ, 94, 1423
Foltz, C. B., Chaffee, F. H., Hewett, P. C., Weymann, R. J., Anderson, S. F., & MacAlpine, G. M. 1989, AJ, 98, 1989
Franceschini, A., LaFranca, F., Cristiani, S., & Martin-Mirones, J. M. 1994, MNRAS, 269, 683
Francis, P. J., Hewett, P., Foltz, C., Chaffee, F., Weymann, R., & Morris, S. 1991, ApJ, 373, 465
Green, P. J., Anderson, S. F., & Ward, M. J. 1992, MNRAS, 254, 30
Hewett, P. C., et al. 1985, MNRAS, 213, 971
Hewett, P. C., Foltz, C. B., & Chaffee, F. H. 1995, AJ, submitted
Hewett, P. C., Foltz, C. B., Chaffee, F. H., Francis, P. J., Weymann, R. J., Morris, S. L., Anderson, S. F., & MacAlpine, G. M. 1991, AJ, 101, 1121
Hooper, E., Impey, C. D., Foltz, C., & Hewett, P. 1995, ApJ, 445, 62
Irwin, M. J., & Trimble, V. 1984, AJ, 89, 93
Isobe, T., Feigelson, E. D., & Nelson, P. I. 1986, ApJ, 306, 490
Jefferys, W. H., Fitzpatrick, M. J., & McArthur, B. E. 1988a, Celest. Mech., 41, 39
Jefferys, W. H., Fitzpatrick, M. J., McArthur, B. E., & McCartnee, J. E. 1988b, GaussFit (computer program; available from W. H. Jefferys, Dept. of Astronomy, Univ. of Texas, Austin, TX 78712)
Kellerman, K. I., Sramek, R., Schmidt, M., Shafer, D. B., & Green, R. 1989, AJ, 98, 1195
Kendall, M., & Stuart, A. 1976, The Advance Theory of Statistics, Vol. II (New York: Macmillan)
Koo, D. C., Kron, R. G., & Cudworth, K. M. 1986, PASP, 98, 285
Kriss, G. A. 1988, ApJ, 324, 809
Krolik, J. H., & Kallman, T. R. 1988, ApJ, 324, 714
Kühr, H., Nauber, U., Paulini-Toth, I. I. K., & Witzel, A. 1979, MPIfR Preprint No. 55
Large, M. I., Mills, B. Y., Little, A. G., Crawford, D. F., & Sutton, J. M. 1981, MNRAS, 194, 693
LaValley, M., Isobe, T., & Feigelson, E. D. 1992, in Astronomical Data Analysis Software and Systems, ed. D. Worrall et al. (San Francisco: ASP), 245
Lawson, A. J., Turner, M. J. L., Williams, O. R., Stewart, G. C., Saxton, R. D., & Lawson, W. A. 1992, MNRAS, 259, 743
Maccacaro, T., Della Ceca, R., Gioia, I. M., Morris, S. L., Stocke, J. T., & Wolter, A. 1991, ApJ, 374, 117
Margon, B., Anderson, S. F., Wu, X., Green, P. J., & Foltz, C. B. 1992, in X-Ray Emission from AGN and the Cosmic X-Ray Background, ed. W. Brinkmann & J. Trümper (Garching: Max Planck), 81
Marshall, H. L., Avni, Y., Braccesi, A., Huchra, J. P., Tananbaum, Zamorani, G., & Zitelli, V. 1984, ApJ, 283, 50
Mathur, S. 1994, ApJ, 431, L75
Mathur, S., Wilkes, B., Elvis, M., & Fiore, F. 1994, ApJ, 434, 493
Morris, S. L., Weymann, R. J., Anderson, S. F., Hewett, P. C., Foltz, C. B., Chaffee, F. H., Francis, P. J., & MacAlpine, G. M. 1991, AJ, 102, 1627
Pfeffermann, E., et al. 1987, Proc. SPIE, 733, 519
Pickering, T. E., Impey, C. D., & Foltz, C. B. 1994, AJ, 108, 1542
ROSAT AO-2 Technical Appendix. 1991, Call for Proposals, MPE Spec. Rept.
Schartel, N., et al. 1995, ApJ, submitted
Schmidt, M., & Green, R. F. 1986, ApJ, 305, 68
Schmitt, J. H. 1985, ApJ, 293, 178 (2KM)
Shanks, T., Georgantopolous, I., Stewart, G. C., Pounds, K. A., Boyle, B. J., & Griffiths, R. E. 1991, Nature, 353, 315
Shastri, P., Wilkes, B. J., Elvis, M., & McDowell, J. C. 1993, ApJ, 410, 29
Stark, A. A., Gammie, C. F., Wilson, R. W., Ballie, J., Linke, R. A., Heiles, C., & Hurwitz, M. 1992, ApJS, 79, 77
Stocke, J. T., et al. 1991, ApJS, 76, 813
Stocke, J. T., Morris, S. L., Gioia, I. M., Maccacaro, T., Schild, R., Wolter, A., Fleming, T., & Henry, J. P. 1992, ApJ, 396, 487
Tananbaum, H., Avni, Y., Green, R. F., Schmidt, M., & Zamorani, G. 1986, ApJ, 305, 57
Trümper, J. 1983, Adv. Space Res., 4, 241
Visnovsky, K. L., Impey, C. D., Foltz, C., Hewett, P., Weymann, R. J., & Morris, S. L. 1992, ApJ, 391, 560
Warren, S. J., Hewett, P. C., & Osmer, P. S. 1994, ApJ, 421, 412
Wilkes, B. J., & Elvis, M. 1987, ApJ, 323, 243
Wilkes, B. J., Tananbaum, H., Worrall, D. M., Avni, Y., Oey, M. S., & Flanagan, J. 1994, ApJS, 92, 53
Worrall, D. M., Giommi, P., Tananbaum, H., & Zamorani, G. 1987, ApJ, 313, 596
Zamorani, G., et al. 1981, ApJ, 245, 357
Zheng, W., & O'Brien, P. T. 1990, ApJ, 353, 433
Zimmermann, H. U., Belloni, T., Izzo, C., Kahabka, P., & Schwentker, O. 1993, EXSAS User's Guide (3d. ed.; München: MPE)